Author(s): Pulkkinen, Tuija I. & Partamies, N. & Kilpua, E. K. J.

Title: Substorm occurrence during quiet solar wind driving

Year: 2014

Version: Final published version

Please cite the original version:

Pulkkinen, Tuija I. & Partamies, N. & Kilpua, E. K. J.. 2014. Substorm occurrence during quiet solar wind driving. Journal of Geophysical Research: Space physics, Vol. 119, nro 4. pp. 2978-2989. ISSN 2169-9402 (electronic). ISSN 2169-9380 (printed). DOI: 10.1002/2013JA019503.

AGU PUBLICATIONS

JGR

Journal of Geophysical Research: Space Physics

RESEARCH ARTICLE

10.1002/2013JA019503

Special Section:
The Causes and Consequences of the Extended Solar Minimum between Solar Cycles 23 and 24

Key Points:
- Substorms do not occur below threshold level of solar wind driving
- Electrojets during solar minimum are weaker than average
- Maximum substorm recurrence during quiet solar activity is 5 h

Correspondence to:
T. I. Pulkkinen,
tuija.pulkkinen@aalto.fi

Citation:
Pulkkinen, T. I., N. Partamies, and E. K. J. Kilpua (2014), Substorm occurrence during quiet solar wind driving, *J. Geophys. Res. Space Physics*, *119*, 2978–2989, doi:10.1002/2013JA019503.

Received 1 OCT 2013
Accepted 28 MAR 2014
Accepted article online 2 APR 2014
Published online 28 APR 2014

Substorm occurrence during quiet solar wind driving

T. I. Pulkkinen[1], N. Partamies[2], and E. K. J. Kilpua[3]

[1]School of Electrical Engineering, Aalto University, Helsinki, Finland, [2]Finnish Meteorological Institute, Helsinki, Finland, [3]Department of Physics, University of Helsinki, Helsinki, Finland

Abstract We examine the OMNI database and International Monitor for Auroral Geomagnetic Effects (IMAGE) magnetometer chain records to study the substorm occurrence and characteristics during quiet solar driving periods, especially during the solar minimum period in 2009. We define substorm-like activations as periods where the hourly average *AL* is below −200 nT. Using the OMNI data set, we demonstrate that there are limiting solar wind speed, interplanetary magnetic field magnitude, and driving electric field values below which substorm-like activations (*AL* < 200 nT, intensification and decay of the electrojet) do not occur. These minimum parameter values are $V < 266$ km/s, $B < 1.4$ nT, and $E < 0.025$ mV/m; such low values are observed less than 1% of the time. We also show that for the same level of driving solar wind electric field, the electrojet intensity is smaller (by few tens of nT), and the electrojet resides farther poleward (by over 1°) during extended quiet solar driving in 2009 than during average solar activity conditions. During the solar minimum period in 2009, we demonstrate that substorm-like activations can be identified from the IMAGE magnetometer chain observations during periods when the hourly average *IL* index is below −100 nT. When the hourly *IL* activity is smaller than that, which covers 87% of the nighttime observations, the electrojet does not show coherent behavior. We thus conclude that substorm recurrence time during very quiet solar wind driving conditions is about 5–8 h, which is almost double that of the average solar activity conditions.

1. Introduction

Magnetospheric substorms are an empirically defined class of dynamic events during which the magnetospheric magnetic field is reconfigured from highly stretched taillike configuration to a quasi-dipolar one [*Baker et al.*, 1996]. In the auroral zone these events are characterized by bright auroral displays and enhanced electrojet currents in the midnight sector [*Akasofu*, 1964]. Substorms, as well as other types of magnetospheric activity, are driven by the solar wind and interplanetary magnetic field (IMF). Solar wind energy enters the magnetosphere through a reconnection process at the boundary when the interplanetary field is antiparallel to the Earth's internal dipole field [*Burton et al.*, 1975]. The magnetotail reconfiguration is a manifestation of another reconnection process, which follows an energy-loading period and slow evolution toward an unstable state [*Hones et al.*, 1986]. Magnetic reconnection onset and the following magnetic field reconfiguration are associated with field-aligned currents that feed current into and out of the ionosphere, thus coupling the magnetospheric dynamic process with the auroral ionosphere [*McPherron et al.*, 1973]. The significance of the substorm as a space physics phenomenon is that it is the dominant way by which the magnetosphere processes energy entering from the solar wind.

The solar wind is highly variable, and substorms occur in many realizations and under a variety of conditions. The complexity of the system and the scarcity of observations during any individual event has made it difficult to quantify the exact nature of the solar wind-magnetosphere coupling as well as the exact correlation of the solar wind parameters and the ionospheric response. Statistically, it has been shown that substorms are more numerous and more intense during high level of solar wind and IMF driving [*Tanskanen*, 2009], and over long timescales there is a good correlation between auroral activity and ionospheric current intensity with the solar cycle phase and level of solar activity [*Nevanlinna and Pulkkinen*, 1998].

Substorms are traditionally identified from the auroral electrojet (*AL*) data as sharp intensifications followed by intensified activity and a slower recovery [*McPherron*, 1991]. Typical duration of the substorm expansion phase (increasing electrojet intensity) is about 30 min, while the recovery phase with decreasing electrojet current is slower, lasting from 1 h up to 3 h [*Pulkkinen et al.*, 1994]. During slow solar wind driving

conditions, the substorms are smaller in intensity and have shorter duration [*Tanskanen et al.*, 2002]. Statistically, substorms recur at about 3 h intervals [*Borovsky et al.*, 1993].

As substorms may overlap—new expansion phase begins before the recovery phase of the previous substorm has ended—and have highly variable realizations, they cannot always be unambiguously defined. Furthermore, there is no rigorous definition of a substorm—the definition is based on phenomenological understanding of a sequence of events, which complicates analysis of either very small or very large substorms. *Rostoker et al.* [1980] discuss the difficulty of setting any size limits to substorms; their size can vary from several thousand nT during magnetic storms to only a few tens of nT during weak solar wind driving. Other authors have considered small activations and termed them "pseudobreakups" arguing that they are isolated auroral activations rather than major reconfiguration or energy dissipation events [e.g. *Koskinen et al.*, 1993]. In order to avoid problems associated with substorm definition, in this study we select an arbitrary limit for the hourly value of the *AL* index of −200 nT to distinguish "active" ionospheric response, which we hypothesize contains substorm activity.

Using the hourly limit value of −200 nT can be justified in two complementary ways: *Akasofu* [1981] defined the ϵ parameter to describe the energy input from the solar wind to the magnetosphere. He argued that the level of energy input of $\epsilon \sim 10^{11}$W is typically required for substorms to occur, while an order of magnitude larger energy input is needed for magnetic storms to develop. *Ahn et al.* [1983] argue that energy dissipation in the ionosphere can roughly be estimated using the *AL* index from $U_I = 3.8 \cdot 10^8 \cdot$ AL [W]. This would indicate that if all the energy input would be dissipated in the ionosphere, this would cause *AL* intensification at most slightly below −200 nT. On the other hand, in a significant statistical study, *Kissinger et al.* [2012] analyze 3000 steady magnetospheric convection events and conclude that typically during these periods with enhanced activity but no clear substorm signatures, the average *AL* was about −200 nT. Thus, the magnetosphere-ionosphere system is capable of maintaining continuous activity without substorms up to about 200 nT activity level. We note that even if using a limiting *AL* value is not a perfect identifier of phenomenologically defined substorms, it picks events that deposit a significant amount of energy into the ionosphere and most likely leaves only a small portion of substorms outside the analysis.

During the recent solar minimum the Sun was very quiet, and the solar wind was weak and steady over an extended time period. This offers a unique opportunity to look at the "ground state" properties of the magnetosphere. In this paper we seek answer to the following questions: (1) Are there threshold values for solar wind driver conditions for substorm occurrence? (2) Is the solar wind-magnetosphere coupling independent of solar activity; especially, is the coupling different during extended solar quiescence? The analysis utilizes the OMNI data covering the solar wind and magnetic activity parameters over the past solar cycle as well as the International Monitor for Auroral Geomagnetic Effects (IMAGE) magnetometer chain data providing latitude-resolved electrojet intensities in a limited local time sector but covering over one solar cycle period.

2. Data

The solar wind driver properties and auroral electrojet indices based on ground-based magnetic recordings were analyzed using the OMNI data set compiled at National Space Science Data Center (http://spdf.gsfc.nasa.gov/). The data set provides hourly averages (1963–2013) and 1 min averages (1995–2013) of the solar wind plasma density and velocity, the interplanetary magnetic field, and the auroral electrojet indices. Especially, the early time periods contain data gaps, while during the later years after 1990s the data set is almost continuous. The upstream observations come from a variety of spacecraft; time delays from the satellite position to the subsolar magnetopause are accounted for by appropriate propagation of the observations (see *King* [2005] for data processing and propagation methods). Figure 1 (left column) shows the sunspot number *R* together with monthly averages of the solar wind density and speed and interplanetary magnetic field intensity at Earth orbit.

Figure 1 (bottom, left) shows the solar wind electric field $E_{\mathrm{PAR}} = E \sin(\theta/2)$, where E is the magnitude of the solar wind electric field computed as $-\mathbf{V} \times \mathbf{B}$ and θ is the IMF clock angle defined as $\theta = \tan^{-1}(B_Y/B_Z)$. The component E_{PAR} gives the electric field component roughly along the large-scale reconnection line at the magnetopause and thus is a measure of the reconnection efficiency at the dayside magnetopause [*Pulkkinen et al.*, 2008; *Laitinen et al.*, 2007]. As the IMF and solar wind speed vary significantly during the 1 h averaging period, the electric field cannot be computed as a product of the 1 h averages of the speed

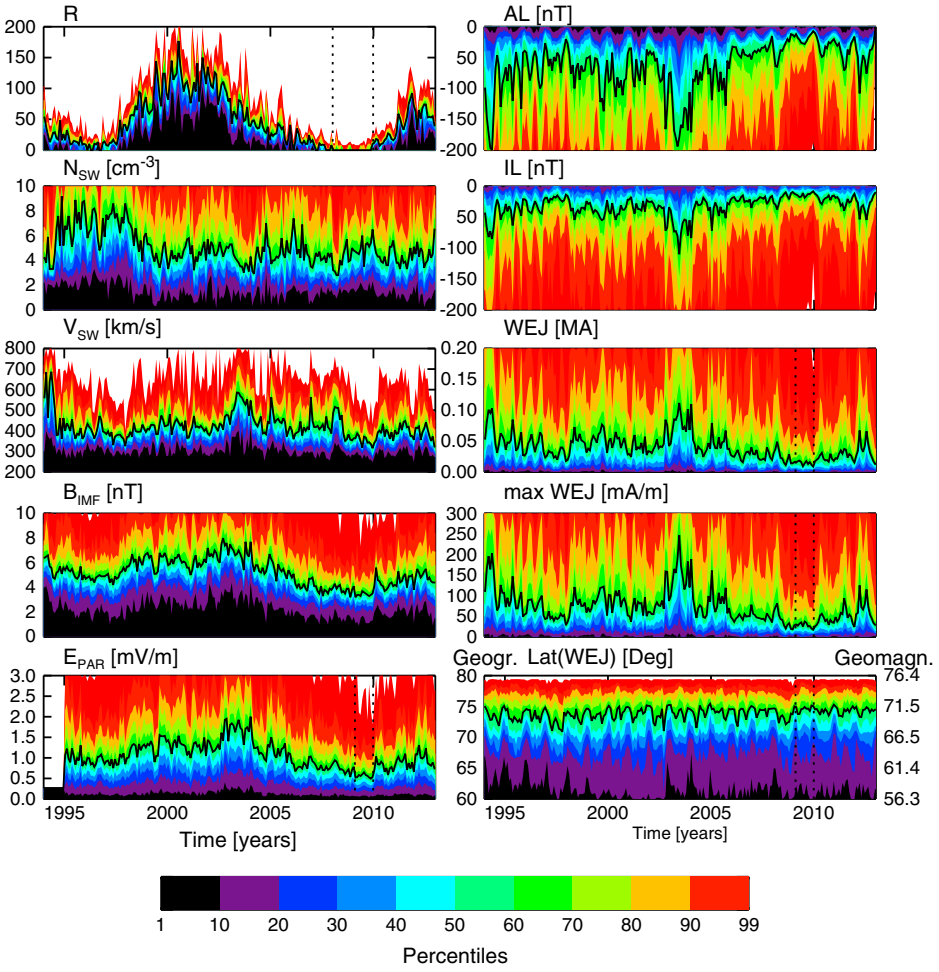

Figure 1. (left column) Drivers of geomagnetic activity: sunspot number *R*, solar wind density *N*, solar wind speed *V*, interplanetary magnetic field intensity *B*, and parallel component of the interplanetary electric field E_{PAR}. All data come from the hourly averaged OMNI data set except the E_{PAR} values computed from the 1 min averaged data set (available only after 1995). The black line shows the median value. (right column) Auroral electrojet response to the solar wind driving: *AL* and *IL* indices, midnight sector total current in the westward electrojet, maximum westward electrojet current density, and central latitude of the westward electrojet (geographic coordinates given in the left axis, corrected geomagnetic coordinates in the right axis). *AL* data come from the OMNI hourly database and the electrojet indices from hourly averages of the IMAGE magnetometer chain measurements. The data format is the same as in the left column.

and IMF magnitude. Therefore, we have used the 1 min files available during 1995–2012 (including 2012) to compute 1 min values for the E_{PAR} and averaged those to hourly values shown in Figure 1 (bottom, left). This is also the reason the analysis below is limited to the period 1995–2012 whenever correlations with the driving electric field are considered.

The vertical dotted lines in Figure 1 (top, left) bracket the most quiet interval with monthly sunspot number less than 5 and daily sunspot number less than 15, from 2008.02 to 2009.98. The vertical lines in Figure 1 (bottom, left) identify the most quiet interval in terms of the driving electric field, from 2009.10 to 2009.98. The latter period will be analyzed in more detail below.

The *AE* station network consists of 12 stations distributed along the northern polar auroral region. While it provides good local time coverage, its latitudinal coverage is limited to single latitude at any given local time, and hence, the magnitude of events occurring at atypically far poleward or equatorward are underestimated. In order to gain information about the latitudinal coverage and more accurate intensity determination of the auroral activations, we complement the global OMNI data set with the IMAGE magnetometer chain measurements. The IMAGE magnetometer network consists of 31 magnetometer stations maintained by 10 institutes from Estonia, Finland, Germany, Norway, Poland, Russia, and Sweden. The long

profile covering geographic latitudes from 58 to 79° geographic latitude (from Tartu in Estonia to Ny Alesund in Svalbard) and roughly between 10 and 30° eastern longitude is especially favorable for electrojet studies. The IMAGE magnetometer network records variations in the geomagnetic field at 10 s cadence. The data are processed in a way analogous to the auroral electrojet upper and lower (*AU*, *AL*) indices to produce local IU/IL indices at 1-min temporal resolution [*Tanskanen et al.*, 2002].

While the indices can be computed for all local times, the *IL* index has been shown to correlate well with the global *AL* index on average in the local time sector 20–04 magnetic local time (MLT), which corresponds to 18–02 UT [*Kauristie et al.*, 1996]. This local time of good correlation depends on the magnitude of the disturbance: larger activity can be observed farther away, while weaker activity requires observations closer to the longitude where the currents flow. When the IMAGE chain is close to local midnight, due to the latitudinal coverage of the network, the *IL* index gives a better indication of the substorm intensity. Similarly, the eastward electrojet response to the *IU* index is clearly visible only when the network is in the dusk sector, roughly 16–20 UT. In the following, we limit the analysis of the westward electrojet using the IMAGE chain to 18–02 UT to ensure that the IMAGE chain is accurately capturing the level of auroral electrojet activity.

Amm and Viljanen [1999] developed a method of characteristics for separating the external magnetic disturbance and calculation of the ionospheric equivalent currents. Using this methodology and the latitudinal coverage of the IMAGE magnetometer chain observations, we compute the latitudinal profile of the equivalent current density in the auroral zone. The maximum current density and the latitude of the maximum value are used to characterize the location and magnitude of the peak current. The total current in the westward electrojet flowing through the network longitude is calculated by integration of the current profile over the range of latitudes.

Tanskanen [2009] developed an automated system to detect substorms using a rapid decrease in the *IL* index as an event trigger. Analysis of the event statistics led the author to discard events that had peak amplitudes less than $IL = -100$ nT. We use the same peak amplitude criterion in our analysis.

The *AL* and *IL* data sets complement each other: While the *AL* index has good longitudinal coverage, it underestimates activity outside the auroral zone as there are no stations at subauroral or polar cap latitudes. In our analysis focusing on a quiet period and weak events, this poses a problem: it is difficult to know whether weak or missing *AL* response is due to missing electrojet current or poorly located recording station. However, substorm-size events ($AL \sim -200$ nT) are associated with currents that typically occur close to the *AE* station latitudes and thus can be remotely sensed from the location of the *AL* stations. Thus, even during quiet periods, the *AL* index gives a good indication of the ionospheric energy dissipation. On the other hand, the IMAGE magnetometer chain covers latitudes from 55 to 75° magnetic latitude and thus can record most auroral zone nightside activations. Due to its limited local time coverage, the IMAGE chain observations can be used only during 30% of the time to ensure that the chain is not too far from the local midnight to give a good recording of the maximum amplitude. However, even using only 30% of the time, the data set is quite a substantial one and allows us to draw conclusions about the statistical behavior of the solar wind-ionosphere coupling.

For the statistical analysis, we use the following averages of the electrojet parameters: the total westward current in the midnight sector, the maximum current density, the latitude of the maximum current density, and the *IL* index. Figure 1 (right column) shows the ionospheric response to the solar wind driving: monthly averages of the *AE* index, the midnight sector (22–02 LT) *IL* index, westward electrojet current, maximum current density, and westward electrojet latitude. The averages shown are computed from 1 min data only during times when the IMAGE chain was in the midnight sector (22–02 LT; note that this is even more stringent condition than the local time limitation to 18–02 discussed above). Comparison of the left and right columns of Figure 1 reveals immediately that even during very low solar activity in 2008–2009, the electrojet current activity did not vanish although it was weaker and resided at higher latitudes than during other times. The electrojet latitude median values are less affected by the quiet solar driving, but the latitude range is substantially smaller during the solar minimum period.

3. Substorms During Weak Solar Wind Driver Parameter Values

First, we seek to answer the question whether substorms occur at all values of solar wind parameters. To that end, we plot in Figure 2 (middle row) the *AL* data as function of sunspot number, solar wind density, speed,

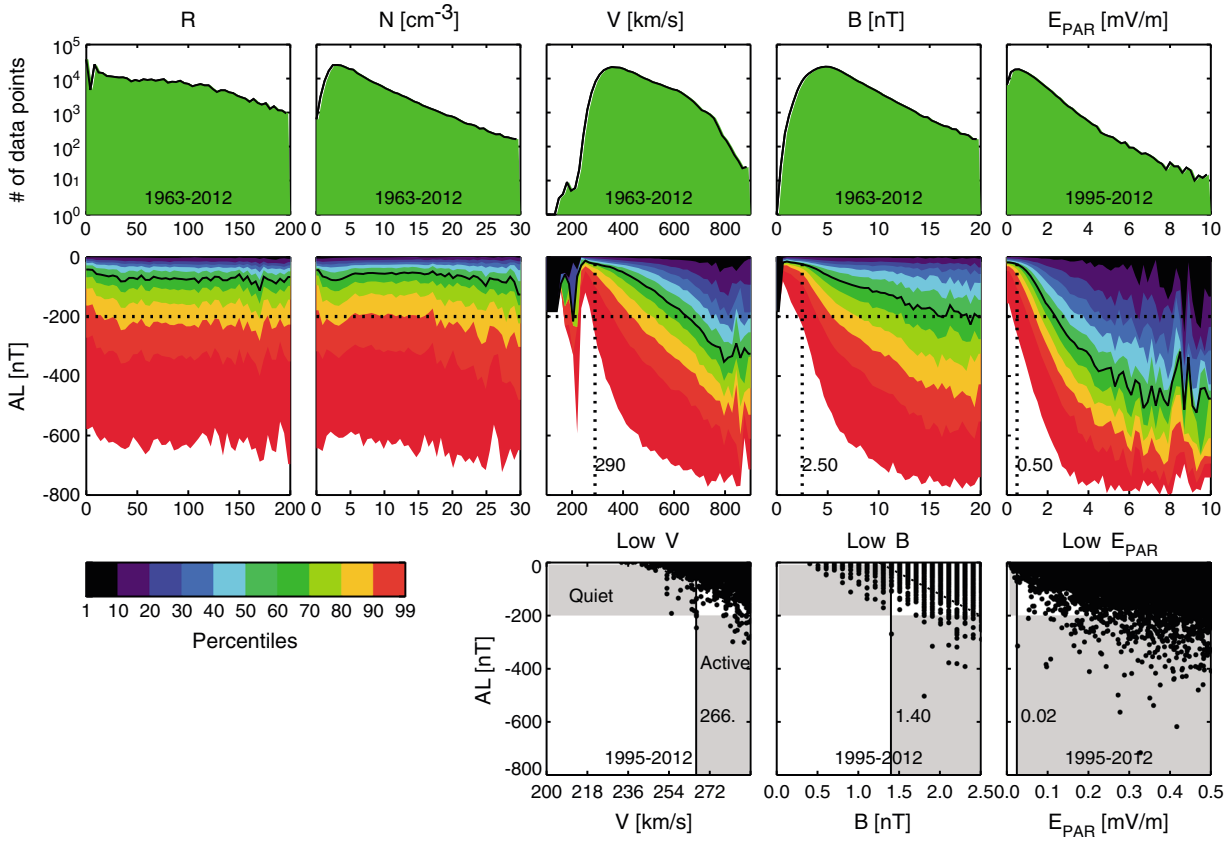

Figure 2. Correlation of *AL* activity with solar wind driver parameters: (top row) number of data points in the hourly averaged OMNI data set (1963–2012) as function of the sunspot number, solar wind density, speed, IMF magnitude, and parallel electric field (limited to 1995–2012). (middle row) *AL* activity as function of the sunspot number, solar wind density, speed, IMF magnitude, and parallel electric field. The black line shows the median value; the color coding shows the percentiles in a format similar to Figure 1. (bottom row) Scatterplots of *AL* versus solar wind speed, IMF magnitude, and parallel electric field (green) for the period 1995–2012. The gray shading identifies the Quiet and Active events analyzed in Figure 3.

interplanetary magnetic field, and parallel electric field. The data come from the hourly averaged OMNI data set using the full-time period 1963–2013. It is evident that the sunspot number or solar wind density do not organize the *AL* observations in a significant way, although the activity is generally higher for very high values of solar wind density. On the other hand, the solar wind speed, interplanetary magnetic field, and electric field show a clear correlation with low *AL* activity at low values of the driver parameters. The limit values at which only 1% of the *AL* observations exceed −200 nT are indicated with black vertical lines with the approximate values next to the line. Figure 2 (top row) shows the number of data points as function of the driver parameters—it is clear that very low values of solar wind speed or IMF magnitude occur only rarely, while low values of driving electric field are frequently observed.

Figure 2 (bottom row) shows values from 1995 onward when also the electric field values are available. The range of driver parameter values shows only the values to the limiting value of the 99th percentile shown in the middle row. Data are shown in a scatterplot format with each hourly value pair indicated with a dot. It is clearly seen that also in this format, the driver versus response has a roughly monotonically decreasing envelope with lower driving producing lower response in the ionosphere.

For each of the driver parameters, we identify the value below which there are no recorded *AL* values below −200 nT. These values are shown with solid vertical lines with values indicated next to the line. The two limiting values, $AL = -200$ nT and minimum driver at which $AL < -200$ nT are observed, divide each plot into four quadrants. Next, we examine two of these quadrants separately: the "Quiet" events with $AL > -200$ nT and driver values below the limit value and the "Active" events with $AL < -200$ nT and driver values above the limit value but within 1% of the lowest driving values. These quadrants are indicated with light gray shading in each panel and labeled in the first panel.

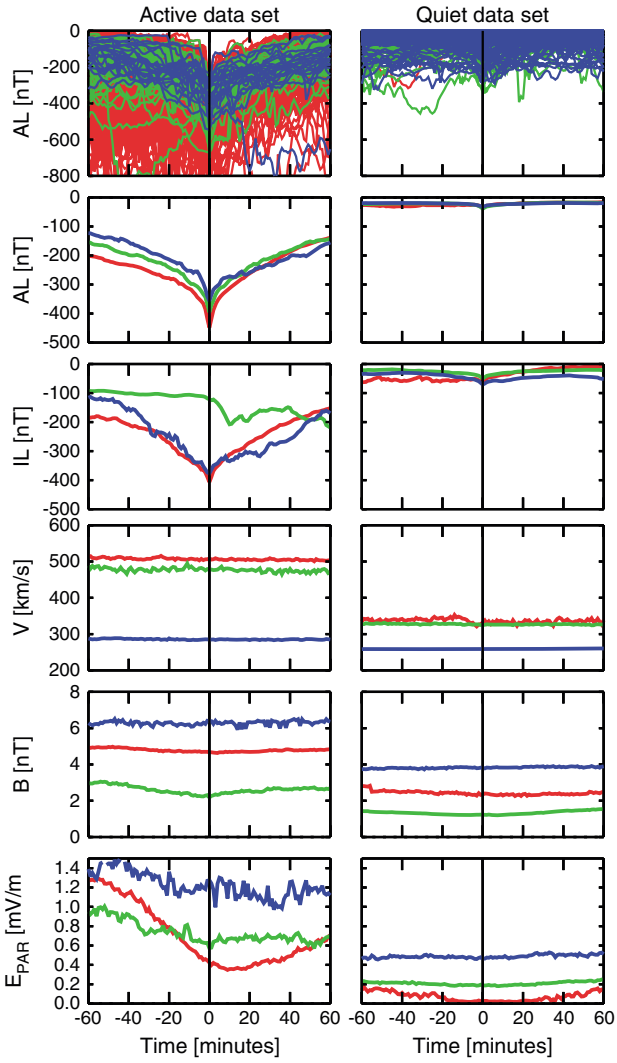

Figure 3. Superposed epoch analysis of (left column) Active and (right column) Quiet events (for definition, see text in section 3). From top to bottom: individual events *AL* index ±60 min from minimum *AL* recording, superposed epoch values for *AL* and *IL*, solar wind speed, IMF magnitude, and parallel electric field E_{PAR}. The three curves in each panel indicate the three different data sets shown in Figure 2 (bottom row) with low solar wind *V* (blue), low IMF *B* (green), and low E_{PAR} (red).

The Quiet events contains 336 measurements with $V < 266$ km/s, 466 measurements with $B < 1.4$ nT, and 37 measurements with $E_{PAR} < 0.025$ mV/m, all with $AL > -200$ nT. The Active data set contains 22 measurements with $266 < V < 290$ km/s, 54 measurements with $1.4 < B < 2.5$ nT, and 407 measurements with $0.025 < E_{PAR} < 0.5$ mV/m, all with $AL < -200$ nT. Next, we examine these two data sets separately to see whether they pose different statistical characteristics.

Figure 3 shows a superposed epoch analysis of the Active and Quiet events using 1 min values of the parameters. The zero time of the superposed epoch was selected as the time when the minimum *AL* value of the hour of observation was reached. The superposition covers the time 60 min before and 60 min after the *AL* minimum time. As two event categories (Active and Quiet) were identified for three driver parameters (low solar wind speed, low IMF magnitude, and low E_{PAR}), in total six different data sets were created. Figure 3 (top row) shows the *AL* index for the individual events for each of the six data sets. The following panels show the superposed epoch *AL* index, superposed epoch *IL* index for events where it was available, solar wind speed, IMF magnitude, and parallel electric field E_{PAR}. The left column shows the Active events for the three data sets with low speed in blue, low IMF *B* in green, and low E_{PAR} in red. The right column shows the Quiet events in a similar format and color coding.

Examination of the first and second panels in the left column (Active events) reveals that these periods show a coherent electrojet activation with lower activity prior to and after the epoch zero time. The superposed epoch curves are quite symmetric, unlike the typical substorm electrojet profile in an individual event with rapid decrease and slow recovery. However, this is a typical superposed epoch result when the substorm epoch zero time is selected to be the activity maximum rather than the activity onset time. Thus, one can conclude that these events are substorms or substorm-like activations.

Figure 3 (right column) shows the Quiet events in the same format. The first panel demonstrates that for individual data points, *AL* values below −200 nT are recorded, while the selection criterion maintains that the hourly average must be above that limit. On the other hand, the superposition shows that the average activity is very low and that there is no structure in the electrojet response; the peak time shows no different electrojet values to the adjacent times.

The *IL* index analysis was limited to cases when the chain was near local midnight (22–02 LT). This limits the number of events such that the low IMF *B* and low speed data sets in the Active data set only had three

and five events, respectively. However, even these small data sets reveal behavior similar to the larger *AL* data set.

The following panels show the superpositions of the driver parameters. The solar wind speed is low only in the data set where it was a selection criterion (low V, shown in blue), while the other two data sets (low B shown in green, low E_{PAR} shown in red) show results quite similar to each other: Quite typical solar wind speed values between 400 and 500 km/s for the Active events, much lower values between 300 and 400 km/s for the Quiet events.

The IMF magnitude is smallest for the data set where it was a selection criterion (low B, shown in green). The data set with low solar wind speed show the highest field magnitudes (low V, shown in blue) the low E_{PAR} data set (shown in red) has average field magnitude above 4 nT for the Active events. While the values are again lower for the Quiet events, the ordering of the curves is similar to the Active events.

The driving electric field E_{PAR} results show that for the low solar wind speed data set (blue), the driving is not necessarily very low (above 1.5 mV/m for the Active events), while for the other two data sets the driving is below 1 mV/m. For comparison, for average solar wind parameters ($V = 400$ km/s, $B = 5$ nT) the electric field is $E = 2$ mV/m. For the Quiet events, the values of the driving electric field are quite low for all data sets.

The conclusion from this analysis is that we can find a threshold value for all major solar wind driver parameters (solar wind speed, IMF magnitude, and driving electric field) below which substorms do not occur: Superposition of these events shows no coherent electrojet response. On the other hand, increasing the driver parameters just slightly above the threshold (even the Active events are in the lowest 1% of the driver parameter values), periods where hourly *AL* activity below −200 nT is observed, shows typical substorm characteristics.

Driver values for which substorms or substorm-like activations do not occur in this comprehensive data set are $V < 266$ km/s, $B < 1.4$ nT, and $E < 0.025$ mV/m.

4. Substorms During Quiet Solar Activity

For a quiet interval, we selected the period around the solar minimum between cycles 23 and 24 during which the daily sunspot number was below 15 and the monthly sunspot number was less than 5 and during which the electric field was at its lowest level (see Figure 1). Figure 4 (left column) shows this interval 2009.1–2009.98 in a format similar to Figure 1 using hourly averages of the IMAGE magnetometer recordings. Note that the data set contains only measurements in the local night sector, during 18–02 UT corresponding to 20–04 MLT. The summer maximum of the westward electrojet intensity is very clear. On the other hand, the electrojet latitude does not show the semiannual minima during fall and spring as clearly as it is observed during more average conditions [*Pulkkinen et al.*, 2011]. All in all, the median of the *IL* index is very low being above -100 nT, and 99% of the time the activity is above −400 nT. Thus, large activations are almost completely missing, and the median activity in the midnight sector is at very low level.

Figure 4 (middle column) shows the electrojet parameters as function of the parallel electric field E_{PAR}. For comparison, Figure 4 (right column) shows the electrojet activity as function of E_{PAR} for the entire data set covering the period from 1995 to 2013. During quiet solar activity, the overall level of driving is low, and E_{PAR} is mostly below 4 mV/m, while under average solar activity conditions values up to 10 mV/m are frequently observed.

Comparison of the middle and right columns allows us to examine the efficiency of the solar wind driving under solar minimum conditions and during average conditions. Horizontal lines showing $IL = -100$ nT and −200 nT and E_{PAR} values of 1 and 2 mV/m are shown to guide the eye: During 2009, about half of the events driven with $E_{PAR} = 2$ mV/m have *IL* index lower than −100 nT, while during the entire period from 1994 to 2012, 2 mV/m driving produced activity in excess of −100 nT over 60% of the time. The insert figure in the lower right corner highlights the lower level of driving during the minimum period in 2009. The graphs show the mean values of the electrojet intensity for both the minimum period (in black) and the entire period 1994–2013 (in red). The thick vertical bars show the variances in each bin indicating that the difference between the two curves for values lower than 1 mV/m is larger than the variance in each data set.

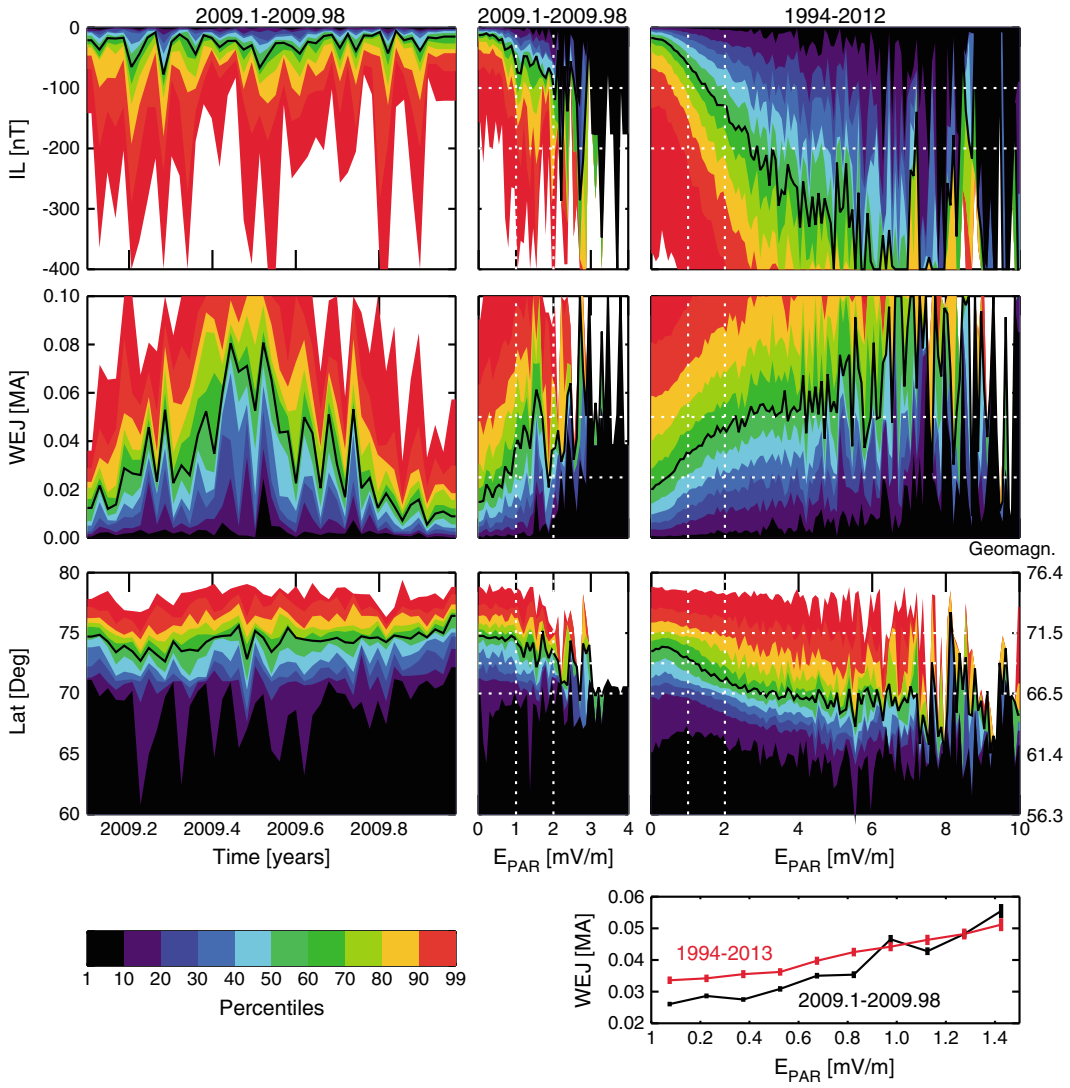

Figure 4. IMAGE magnetometer chain observations. (left column) The *IL* index, westward electrojet intensity, and latitude as function of time during the quiet solar activity interval 2009.1–2009.98. (middle column) The *IL* index, westward electrojet intensity, and latitude as function of driving parallel electric field E_{PAR} during the quiet solar activity interval 2009.1–2009.98. (right column) The *IL* index, westward electrojet intensity, and latitude (geographic coordinates given in the left axis, corrected geomagnetic coordinates in the right axis) as function of driving parallel electric field E_{PAR} during 1994–2013. The insert figure in the bottom right corner shows the average values of the westward electrojet intensity for the period 2009.1-2009.98 in black and 1994–2012 in red, as a function of the parallel electric fields. The thick bars show the variance within each bin.

Significant differences are seen in the electrojet latitude: During 2009, for low levels of driving $E_{PAR} < 1$ mV/m, the electrojet median is close to 75° latitude, while it is over 1° farther equatorward during average conditions. For moderate driving $1 < E_{PAR} < 2$ mV/m the difference is several degrees in the median values. The few occasions of higher level of driving during 2009 rarely bring the electrojet to values below 70°, which is the median for the more average driving conditions. Thus, we conclude that during the extended period of weak driving in 2009, the ionospheric response to solar wind driving was weaker than during average conditions: For the same level of driving electric field, the electrojet current was weaker, and it was located farther poleward in 2009 than during 1994–2012.

For the data set covering the period 2009.1–2009.98, we selected periods with the hourly average activity in the range of $IL < -200$ nT (116 hourly data points), $-200 < IL < -100$ nT (254 hourly data points), and $-100 < IL < 0$ nT (2114 hourly data points). For these times, we examined the 1 min *IL* records and identified the minimum value during each hour. Using the times of the minimum value in the 1 min data set,

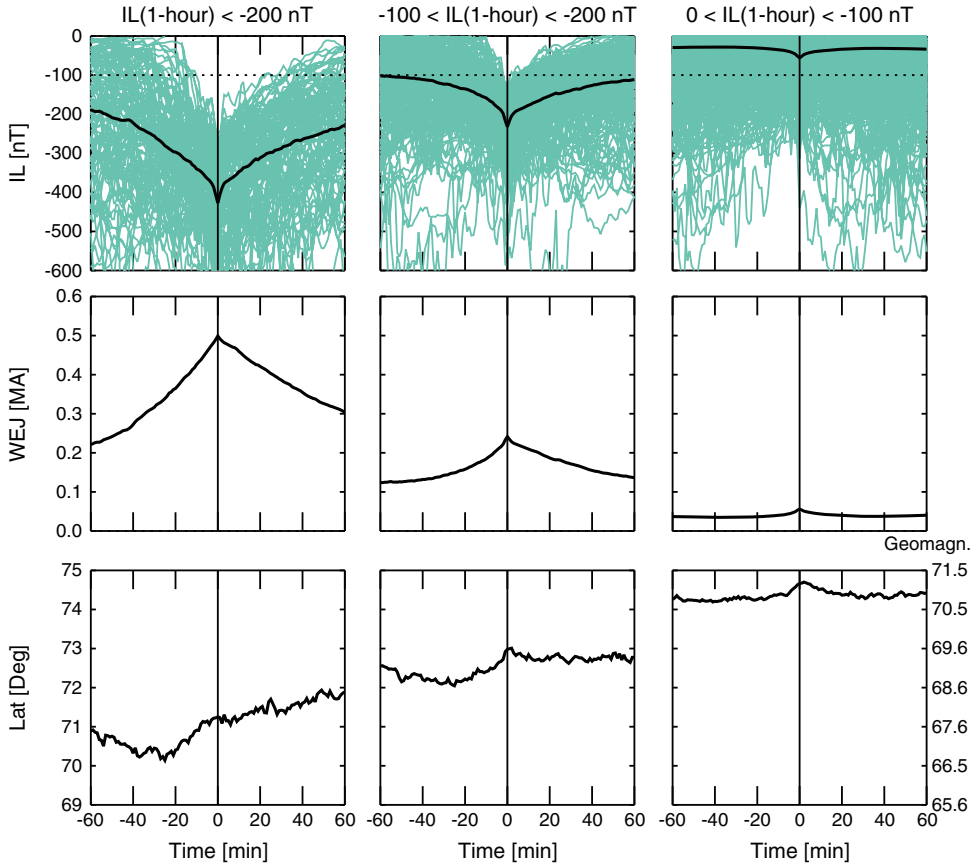

Figure 5. Superposed epoch analysis of IMAGE magnetometer chain observations during quiet solar activity interval 2009.1–2009.98, (top row) *IL* index, (middle row) westward electrojet intensity, and (bottom row) electrojet latitude (geographic coordinates given in the left axis, corrected geomagnetic coordinates in the right axis). Hourly average of (left column) $IL < -200$ nT, (middle column) $-200 < IL < -100$ nT, and (right column) $-100 < IL < 0$ nT.

we constructed a time series with 60 min prior to the minimum and 60 min after the minimum value. These time series were then used to create superposed epoch curves shown in Figure 5.

Figure 5 (top row) shows the *IL* index with individual time series plotted in green and the average shown in black. The middle row shows the westward electrojet current, and the bottom row shows the latitude of the westward electrojet center. As the events were selected based on the *IL* response, it is not surprising that both the *IL* index and the westward electrojet intensity show a clear ordering in intensity. Furthermore, it is very clear that the electrojet latitude moves poleward as the level of electrojet intensity decreases.

The two first categories, $IL < -200$ nT and $-200 < IL < -100$ nT, in the left and middle columns show a clear maximum and a coherent behavior of increasing and subsiding activity with respect to the peak activity time. These superposed epoch results with first increasing and then decreasing electrojet activity, equatorward motion of the electrojet prior to the peak activity time followed by a poleward motion and/or higher-latitude location of the peak electrojet current after the peak activity time very much resemble the behavior of the electrojets during substorms. We therefore conclude that these categories mostly contain activity that can be classified as substorms.

On the other hand, the lowest-activity category (right column) does not show such coherent behavior. The *IL* values before and after the peak time are neither smaller nor larger than the peak value; the superposed epoch average is small and does not reveal a structure of increasing and subsiding activity. Due to the lack of coherent structure during individual events or in the superposed epoch curves, we conclude that the lowest-activity category (right column) contains periods with randomly occurring short-duration electrojet activity but not arranged in a coherent sequence. This result further justifies our use of −100 nT as the

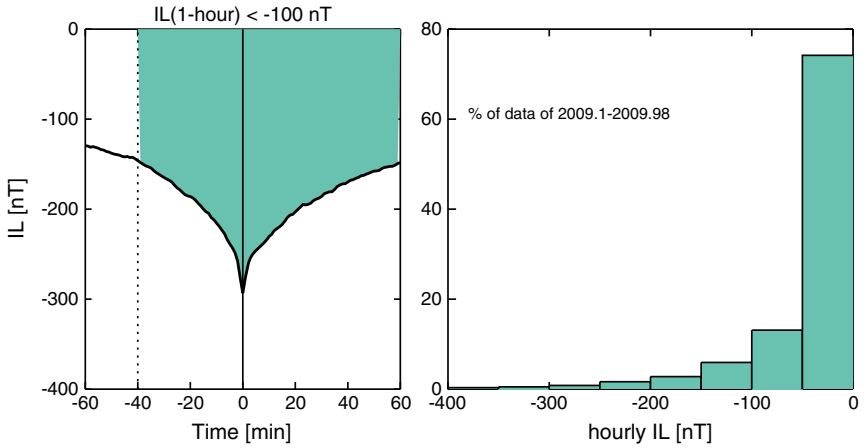

Figure 6. (left) Superposed epoch analysis of IMAGE magnetometer chain observations during quiet solar activity interval 2009.1–2009.98, *IL* index for periods with hourly average of $IL < -100$ nT. (right) Histogram of hourly averages of IMAGE magnetometer chain observations during quiet solar activity interval 2009.1–2009.98 and in the night sector (18–02 UT). The bin size is 50 nT, and the data are shown as percentages of observations falling in each bin.

minimum requirement for substorm activity in the analysis of the IMAGE magnetometer results. The horizontal dashed lines in the top row indicate the −100 nT limit.

These results can further be used to examine the average recurrence time of substorm activity. Figure 6 (left) repeats the analysis in Figure 5 but combining the two left columns. Thus, we get a superposed epoch curve for all periods that we would characterize as substorm-like activity (see discussion above). The shaded area shows the duration during which the *IL* index is more than half of the peak value, which shows that the average duration of the events defined as intensity above half of peak value is about 100 min.

Figure 6 (right) shows a histogram of hourly observations of the *IL* index binned at 50 nT intervals. The number of hourly observations is divided by the total number of the observation hours in the night sector (18–02 UT) during the time period 2009.1–2009.98. This histogram shows that the hourly values are below −100 nT only 13% of the time. These are the periods when one would assume substorms to occur.

Assuming that during each hour of *IL* below −100 nT produces only one substorm, one would get a recurrence rate of one substorm every 8 h. Considering that the activity typically lasts 100 min (Figure 6, left), the recurrence time can be higher up to one substorm every 5 h. Both these numbers are significantly lower than the average of one substorm every 3 h [*Borovsky et al.*, 1993].

Thus, we conclude that substorms have smaller intensity and lower occurrence frequency during the extended solar minimum in 2009 than during more average conditions.

5. Discussion

The solar minimum period between solar cycles 23 and 24 was quite extraordinary: the Sun was very quiet with almost 2 years of near-zero sunspot numbers. Similarly, the solar wind parameters changed significantly from their average values, the solar wind speed was low, the density was quite small, and the IMF magnitude was small. Thus, the period offers a unique opportunity to look at the magnetospheric response to the solar wind driving in a situation where the magnetosphere is close to its ground state.

Substorm studies suffer from the fact that they are empirically defined, and there is no rigorous definition of the phenomenon. While "average" substorms are easier to identify, definitions become highly ambiguous when examining the lower or upper end of the statistics, either very small or large substorms, weak or strong solar wind, and IMF driving conditions. In this study, we concentrate on the lower end of the activity spectrum and examine electrojet activity during weak solar wind and IMF driving conditions. In order to avoid problems associated with defining "what is a substorm," we define "substorm-like activity" to occur when the hourly average of the *AL* index is below −200 nT. We then use superposed epoch analysis to demonstrate that this definition indeed works—the superposed epoch results clearly reproduce the typical

substorm sequence of rising and decaying electrojet intensity over a time period of 2 h when the activity is higher than −200 nT, while there is no coherent response for periods with $AL > -200$ nT.

During quiet solar wind driving, the median values of auroral electrojet activity become low, but the most striking difference is the lack of high values in the distribution. Figure 1 clearly shows that both in the *AL* and *IL* data sets, the solar minimum period is one where large events are almost completely lacking. Furthermore, the electrojet moves farther poleward and loses its semiannual variation for the duration of very low solar activity.

Correlating the *AL* index with the solar wind driver parameters indicates that there are values of solar wind speed, IMF magnitude, and parallel electric field E_{PAR} below which substorm-like coherent electrojet activations (defined here as periods with hourly *AL* less than −200 nT) do not occur. These minimum parameter values are $V < 266$ km/s, $B < 1.4$ nT, and $E < 0.025$ mV/m. While a larger data set might change the details of these numbers, we conclude that the data set is sufficiently large to draw the conclusion that for very low driver values substorm activity disappears and the (weak) energy input is dissipated in continuously and/or during short-term noncoherent activations.

Comparison of the IMAGE magnetometer records and driving solar wind parameters shows that the electrojet is weaker for driving levels smaller than $E_{PAR} < 1$ mV/m and resides at more poleward latitudes during the quiet solar activity period than during average solar activity. This is true also when the low-driving electric field during the solar minimum is accounted for: Organizing the observations according to the driving electric field shows that the electrojet response to the driving solar wind electric field is weaker during quiet solar activity. This would suggest that the efficiency of the solar wind-magnetosphere coupling is not constant but depends on the driver intensity in a way that the efficiency is smaller when the driving is very weak. Note that this result cannot be interpolated to more average solar wind conditions: *Palmroth et al.* [2007] found that during average solar activity conditions, solar wind pressure pulses associated with higher-driving electric field cause relatively smaller ionospheric electrojet response than pressure pulses during which the electric field driving was weak. *Pulkkinen et al.* [2007] examined storm time substorms and concluded that during storm times (high solar wind driving), the ionospheric electrojet response was weaker than during isolated substorms. *Partamies et al.* [2009] show that during steady convection intervals during which the driving electric field is moderate and steady, the ionospheric response is relatively larger than under more active conditions, either magnetic storms or sawtooth events.

Analysis of the IMAGE magnetometer recordings shows that if the hourly *IL* index is below −200 nT, the electrojet shows a clear substorm-like period with intensification and decay of the current over a 2 h period and poleward expansion of the electrojet latitude. Furthermore, in the average intensity range $-200 < IL < -100$ nT, similar features are found although the poleward expansion is not as clear. For weak activity, there is no coherent behavior, and it can be concluded that for periods with hourly average *IL* index above −100 nT, there are no substorm-like activations. Turning that into substorm occurrence frequency indicates that the maximum substorm recurrence time even under the quietest solar wind periods is 5 to 8 h. Thus, during extended periods of very low solar wind driving, the substorm occurrence rate drops to almost half of the average of below 3 h, and the events typically are smaller and of shorter duration. This result is qualitatively in agreement with *Partamies et al.* [2013] who conclude that during solar minima, there are longer periods without substorm or storm activity than during other solar activity conditions. Furthermore, they show that during solar minima there are fewer recurrent substorms and that isolated substorms are small in intensity.

6. Summary

1. The *AL* indices from the OMNI database provide a means to examine the global long-term auroral activity relation to solar wind driving for over four solar cycles from 1963 onward. The 1 min values available since 1994 are needed for accurate evaluation of the driving solar wind electric field, which cannot be correctly computed from the hourly values. The IMAGE magnetometer chain provides, in a limited local time sector, a latitudinally resolved electrojet profile and information about the peak current density, the location of the maximum electrojet current, and the total current in the electrojets. These data are available at 1 min resolution since 1994.
2. There are limit values for solar wind speed, IMF magnitude, and driving electric field below which we do not observe substorm-like activations producing hourly *AL* index values below −200 nT and coherent

intensification and decay of the auroral electrojet. These minimum values are $V < 266$ km/s, $B < 1.4$ nT, and $E < 0.025$ mV/m. Such values are observed less than 1% of the time in the entire hourly OMNI data set.

3. The IMAGE magnetometer results show that the electrojets are weaker (for driving levels smaller than $E_{PAR} < 1$ mV/m) and reside farther poleward during quiet solar driving than during average solar activity conditions for the same level of driving solar wind electric field. Differences in the hourly *IL* values are few tens of nT and over 1° in latitude.
4. The IMAGE magnetometer results show that coherent substorm-like activations can be identified during periods when the hourly average *IL* index is below −100 nT, which is the limiting value used also in earlier studies. When the hourly *IL* activity is smaller than −100 nT, the electrojet does not show coherent behavior, and such conditions during 2009 prevail 87% of the time. During these very quiet solar wind driving conditions, substorm recurrence time is thus about 5–8 h, which is almost double that of the average solar activity conditions.

Acknowledgments

The work of T.I. Pulkkinen and E.K.J. Kilpua has been supported by the Academy of Finland. We thank the organizers of the Chapman Conference on Causes and Consequences of the Extended Solar Minimum Between Solar Cycles 23 and 24 (4CESM) for the invitation to speak at the meeting, which prompted this study.

Masaki Fujimoto thanks the reviewers for their assistance in evaluating this paper.

References

Ahn, B.-H., S.-I. Akasofu, and Y. Kamide (1983), The Joule heat production rate and particle energy injection rate as a function of the geomagnetic indices AE and AL, *J. Geophys. Res.*, *88*, 6275–6287, doi:10.1029/JA088iA08p06275.

Akasofu, S.-I. (1964), The development of the auroral substorm, *Planet. Space Sci.*, *12*, 273–282.

Akasofu, S.-I. (1981), Energy coupling between the solar wind and the magnetosphere, *Space Sci. Rev.*, *28*, 121–190.

Amm, O., and A. Viljanen (1999), Ionospheric disturbance magnetic field continuation from the ground to the ionosphere using spherical elementary current systems, *Earth Planets Space*, *51*, 431–440.

Baker, D. N., T. I. Pulkkinen, V. Angelopoulos, W. Baumjohann, and R. L. McPherron (1996), Neutral line model of substorms: Past results and present view, *J. Geophys. Res.*, *101*, 12975–13010, doi:10.1029/95JA03753.

Borovsky, J. E., R. J. Nemzek, and R. D. Belian (1993), The occurrence rate of magnetospheric-substorm onsets: Random and periodic substorms, *J. Geophys. Res.*, *98*, 3807–3813, doi:10.1029/92JA02556.

Burton, R. K., R. L. McPherron, and C. T. Russell (1975), An empirical relationship between interplanetary conditions and Dst, *J. Geophys. Res.*, *80*, 4204–4214.

Hones, E. W. J., T. A. Fritz, J. Birn, J. Cooney, and S. J. Bame (1986), Detailed observations of the plasma sheet during a substorm on April 24, 1979, *J. Geophys. Res.*, *91*, 6845–6859, doi:10.1029/JA091iA06p06845.

Kauristie, K., T. I. Pulkkinen, R. J. Pellinen, and H. J. Opgenoorth (1996), What can we tell about global auroral-electrojet activity from a single meridional magnetometer chain?, *Ann. Geophys.*, *14*, 1177–1185, doi:10.1007/s00585-996-1177-1.

King, J. H. (2005), Solar wind spatial scales in and comparisons of hourly Wind and ACE plasma and magnetic field data, *J. Geophys. Res.*, *110*, A02104, doi:10.1029/2004JA010649.

Kissinger, J., R. L. McPherron, T. S. Hsu, V. Angelopoulos, and X. Chu (2012), Necessity of substorm expansions in the initiation of steady magnetospheric convection, *Geophys. Res. Lett.*, *39*, L15105, doi:10.1029/2012GL052599.

Koskinen, H. E. J., R. E. Lopez, R. J. Pellinen, T. I. Pulkkinen, D. N. Baker, and T. Bosinger (1993), Pseudobreakup and substorm growth phase in the ionosphere and magnetosphere, *J. Geophys. Res.*, *98*, 5801–5813, doi:10.1029/92JA02482.

Laitinen, T. V., M. Palmroth, T. I. Pulkkinen, P. Janhunen, and H. E. J. Koskinen (2007), Continuous reconnection line and pressure-dependent energy conversion on the magnetopause in a global MHD model, *J. Geophys. Res.*, *112*, A11201, doi:10.1029/2007JA012352.

McPherron, R. L. (1991), Physical processes producing magnetospheric substorms and magnetic storms, in *Geomagnetism*, edited by J. A. Jacobs, pp. 593–739, Acad. Press, London.

McPherron, R. L., C. T. Russell, and M. P. Aubry (1973), Satellite studies of magnetospheric substorms on August 15, 1968. IX. Phenomenological of model for substorm, *J. Geophys. Res.*, *78*, 3131–3149.

Nevanlinna, H., and T. I. Pulkkinen (1998), Solar cycle correlations of substorm and auroral occurrence frequency, *Geophys. Res. Lett.*, *25*, 3087–3090, doi:10.1029/98GL02335.

Palmroth, M., et al. (2007), Solar wind-magnetosphere coupling efficiency for solar wind pressure impulses, *Geophys. Res. Lett.*, *34*, L11101, doi:10.1029/2006GL029059.

Partamies, N., T. I. Pulkkinen, R. L. McPherron, K. McWilliams, C. R. Bryant, E. Tanskanen, H. J. Singer, G. D. Reeves, and M. F. Thomsen (2009), Different magnetospheric modes: Solar wind driving and coupling efficiency, *Ann. Geophys.*, *27*, 4281–4291.

Partamies, N., L. Juusola, E. Tanskanen, and K. Kauristie (2013), Statistical properties of substorms during different storm and solar cycle phases, *Ann. Geophys.*, *31*(2), 349–358.

Pulkkinen, T., M. Palmroth, and T. Laitinen (2008), Energy as a tracer of magnetospheric processes: GUMICS-4 global MHD results and observations compared, *J. Atmos. Sol. Terr. Phys.*, *70*(5), 687–707.

Pulkkinen, T. I., D. N. Baker, P. K. Toivanen, R. J. Pellinen, R. H. W. Friedel, and A. Korth (1994), Magnetospheric field and current distributions during the substorm recovery phase, *J. Geophys. Res.*, *99*, 10,955–10,966, doi:10.1029/93JA02718.

Pulkkinen, T. I., C. C. Goodrich, and J. G. Lyon (2007), Solar wind electric field driving of magnetospheric activity: Is it velocity or magnetic field?, *Geophys. Res. Lett.*, *34*, L21101, doi:10.1029/2007GL031011.

Pulkkinen, T. I., E. I. Tanskanen, A. Viljanen, N. Partamies, and K. Kauristie (2011), Auroral electrojets during deep solar minimum at the end of solar cycle 23, *J. Geophys. Res.*, *116*, A04207, doi:10.1029/2010JA016098.

Rostoker, G., S.-I. Akasofu, J. Foster, R. A. Greenwald, Y. Kamide, K. Kawasaki, A. T. Y. Lui, R. L. McPherron, and C. T. Russell (1980), Magnetospheric substorms—Definition and signatures, *J. Geophys. Res.*, *85*, 1663–1668.

Tanskanen, E., T. I. Pulkkinen, H. E. J. Koskinen, and J. A. Slavin (2002), Substorm energy budget during low and high solar activity: 1997 and 1999 compared, *J. Geophys. Res.*, *107*, 1086, doi:10.1029/2001JA900153.

Tanskanen, E. I. (2009), A comprehensive high-throughput analysis of substorms observed by IMAGE magnetometer network: Years 1993–2003 examined, *J. Geophys. Res.*, *114*, A05204, doi:10.1029/2008JA013682.